A Refined Understanding of the Cloud Longwave Scattering Effects in Climate Model

Chongxing Fan[1]*, Yi-Hsuan Chen[1+], Xiuhong Chen[1], Wuyin Lin[2], Ping Yang[3], Xianglei Huang[1]

[1] Department of Climate and Space Sciences and Engineering, the University of Michigan, Ann Arbor, Michigan, USA

[2] Environmental & Climate Sciences Department, Brookhaven National Laboratory, New York State, USA

[3] Department of Atmospheric Sciences, Texas A&M University, Texas, USA

* Corresponding Author: Chongxing Fan (cxfan@umich.edu)

[+] Current affiliation: The Program in Atmospheric and Oceanic Sciences, Princeton University, New Jersey, USA

Key Points

- Including ice cloud LW scattering leads to ~2 W m^{-2} instantaneous OLR reduction in the tropics when compared to other climate zones.
- Strong surface warming in the Arctic after including ice cloud LW scattering is dominantly caused by polar amplification.
- Tropical cloud responses due to cloud LW scattering are similar to those induced by increasing greenhouse gases.

Submitted to *Journal of Advanced Modeling Earth Systems*

Original submission on November 5, 2022

Abstract

Because strong absorption of infrared radiation by greenhouse gases is more significant than the cloud longwave (LW) scattering effect, most climate models neglect cloud LW scattering to save computational costs. However, ignoring cloud LW scattering directly overestimates the outgoing longwave radiation (OLR). A recent study performed slab-ocean model simulations in the Community Earth System Model and showed that such radiative flux changes due to ice cloud LW scattering can affect the polar surface climate more than other climate zones. In this study, we included the same ice cloud LW scattering treatment in the Exascale Energy Earth System Model (E3SM) version 2 and ran fully-coupled simulations to assess the impact of ice cloud LW scattering on global climate simulation. Including ice cloud LW scattering leads to ~2 Wm^{-2} instantaneous OLR reduction in the tropics, more than the OLR reduction in other climate zones. Strong surface warming occurs in the Arctic, which is dominantly caused by the polar amplification resulting from the radiative forcing caused by ice cloud LW scattering. In the tropics, when the ice cloud LW scattering effect is included, more liquid clouds form in the middle troposphere, high clouds in the convection zone are lifted, anvil clouds retreat, and stratiform low cloud fraction increases. Most of these effects are similar to the cloud response to the increase of well-mixed greenhouse gases. The present study suggests that the ice cloud LW scattering effect must be incorporated into climate simulations.

Plain Language Summary

Clouds, like greenhouse gases, can block radiative energy emitted below from reaching the top of the atmosphere by either absorbing it or scattering it elsewhere. Cloud longwave scattering is deemed less important and thus neglected in most climate models to save computational time. We put this mechanism back in a climate model and ran pairs of simulations, with or without cloud scattering, to see how it would affect the simulated global climate. We found that cloud longwave scattering reduces the longwave radiation that goes to space and, consequently, triggers responses of the climate system. Although direct reduction of outgoing longwave radiation is strongest in the tropics, induced warming, as part of the responses, is strongest in the Arctic, similar to how the climate system responds to the increases of greenhouse gases. Furthermore, cloud properties will change, especially in the tropics, after including the cloud longwave scattering process. We argue that cloud longwave scattering is indeed important and should be included in climate simulations.

1. Introduction

Clouds play an important role in the climate system (Stephens, 2005; and references therein). Despite its importance in the climate system, cloud feedbacks still remain the largest uncertainty in climate feedback estimation (Sherwood et al., 2020). This is partly due to the multi-scale complexity of cloud processes, its intricate connections with large-scale dynamics, radiation, and cloud microphysics, and the underrepresentation of known physical processes by the climate models due to various computational constraints.

For example, cloud longwave (LW) scattering is one of such underrepresented physical processes in climate models. The cloud scattering effect is believed to be secondary in the LW due to strong LW absorption by greenhouse gases and clouds. As a result, a dominant majority of climate models neglect the LW scattering to save computational costs. Earlier studies using offline radiative transfer calculation have pointed out that omitting cloud LW scattering can lead to an overestimation of outgoing longwave radiation (OLR) (Stephens, 1980). When considered, scattered photons might be absorbed by greenhouse gas molecules or cloud particles, leading to a different atmospheric radiative cooling rate and, consequently, a different surface downward LW flux (Ritter & Geleyn, 1992). Several parameterization schemes have been proposed to include the multiple scattering of LW fluxes by clouds in the climate models (Chou et al., 1999; Fu et al., 1997; Li & Fu, 2000). Using atmospheric profiles from model simulations or reanalysis, these studies estimated the differences in LW fluxes and atmospheric radiative heating profile due to cirrus LW scattering (Chou et al., 1999; Fu et al., 1997; Joseph & Min, 2003; Ritter & Geleyn, 1992). The

77 instantaneous reduction of OLR ranges from 6~8 W/m^2 depending on atmospheric conditions and
78 the increase in downward LW flux at the surface (FLDS) ranges from 2~4 W/m^2. Aside from cirrus
79 clouds that were believed to induce the most prominent LW scattering effect, there have been
80 published studies stressing the importance of scattering LW fluxes for radiation budget over the
81 marine stratocumulus cloud regions (Costa & Shine, 2006; Kuo et al., 2017; Schmidt et al., 2006).
82 It was estimated that, without LW scattering, the global-mean OLR is overestimated by 1.5~3
83 W/m^2.

84 These studies all focused on the direct impact of cloud scattering on radiation budget. There have
85 been studies to use prescribed-SST simulations to investigate how the cloud LW scattering effect
86 can affect the overall simulated climate (Jin et al., 2019; Zhao et al., 2018). They agreed on the
87 magnitude of global-mean OLR reduction by ~2.6 W/m^2 when considering the effect of cloud LW
88 scattering. Zhao et al. (2018) pointed out that such OLR reduction is amplified by water vapor
89 response to the warming atmosphere, given that the instantaneous global-mean OLR reduction due
90 to scattered LW flux by clouds is 1.8 W/m^2. However, such prescribed-SST simulations cannot
91 evaluate the impact of cloud LW scattering on surface climate as the surface-atmosphere coupling
92 is constrained. To address this, Chen et al. (2020) used the Community Earth System Model
93 (CESM) 1.1 slab-ocean model with a modified LW scheme to study the ice cloud LW scattering
94 effect. They argued that cloud LW scattering is especially important over polar regions due to the
95 small amount of water vapor in such regions. Their simulations showed a 1.0~2.0 K increase in
96 the seasonal-mean surface air temperature over the polar region, which is at least twice as fast as

97 that in the tropics. As a cursory study, Chen et al. (2020) also identified the strong correlations
98 between the polar surface air temperature change and the change of polar surface downward LW
99 flux. However, the analysis by Chen et al. (2020) is largely confined to the polar region without
100 examining possible connections between extra-polar and polar regions (Holland & Bitz, 2003;
101 Stuecker et al., 2018).

102 To the best of our knowledge, no study has used a fully coupled model to study the effect of cloud
103 LW scattering on the simulated climate. In particular, previous modeling studies also limited their
104 scope largely to the surface temperature response and ignored other climate variables like clouds.
105 In this study, we incorporate the same ice-cloud LW scattering treatment in Chen et al. (2020) into
106 the Exascale Energy Earth System Model (E3SM) version 2, a flagship climate model developed
107 by the Department of Energy (Golaz et al., 2022). LW scattering by liquid water clouds is not
108 included here because it is estimated to be much weaker than that by ice clouds (Kuo et al., 2017).
109 Hereafter, cloud LW scattering refers to ice cloud LW scattering only. Using the modified model,
110 we ran fully coupled simulations to investigate changes in radiation budgets, temperature, and
111 cloud in both tropics and polar regions when ice cloud LW scattering is enabled. We also
112 decompose the radiative flux changes into the direct changes caused by the scattering and the
113 indirect changes caused by feedbacks in response to the direct influence of scattering. Section 2
114 describes the model we used and our modifications, as well as the numerical experiments. After a
115 brief discussion of the TOA radiation budget in section 3, section 4 presents a refined

understanding of the cloud LW scattering effect on the temperature response. The cloud response in the tropics is investigated in section 5, followed by a conclusion and discussion section.

2. Model, Data and Methods

2.1. E3SM version 2

E3SMv2 (Golaz et al., 2022) is the successor of the first version of the E3SM model (E3SMv1) developed by the Department of Energy (Golaz et al., 2019). Although the first version was initially branched from CESM1, the second version is very different from CESM as most components have been replaced or heavily modified, including the atmosphere dynamical core, ocean model, sea ice model, and river routing. Atmospheric physics in E3SMv2 still share similarities with CESM2. To evaluate the model, the E3SM team conducted experiments according to a standard set of the Coupled Model Intercomparison Project Phase 6 (CMIP6) Diagnosis, Evaluation, and Characterization of Klima (DECK) simulations (Eyring et al., 2016). Compared to its predecessor, E3SMv2 doubles its speed and alleviates some issues. For example, it simulates better clouds and precipitation climatology and, consequently, improves the estimates of cloud feedbacks and equilibrium climate sensitivity (ECS). While E3SMv1 estimates an ECS of 5.3 K, which is deemed too high, E3SMv2 estimates a more realistic ECS value of 4.0 K.

Our new simulations were branched from different points of the 500-year E3SMv2 pre-industrial control run (v2.LR.piControl), one of the standard runs in the CMIP6 DECK experiment. These simulations run on a horizontal grid of ~100 km in the atmosphere and land components, 1/2-degree in the river component, and 60 to 30 km in the ocean and sea-ice components. The

atmosphere has 72 vertical layers from the surface to approximately 60 km. Note that the model runs on separate dynamics and column parameterization grids to improve computational efficiency. As a result, the dynamics grid has an average horizontal grid of 110 km, while the parameterization grid and the land grid have an average grid size of 165 km.

2.2. Model modifications to enable ice-cloud LW scattering

This study employed the same ice-cloud optics and longwave radiation schemes as described in Chen et al. (2020). In brief, a hybrid two-stream and four-stream (2S/4S) radiative transfer solver is used for longwave radiative transfer so the scattering can be included. Compared to other solvers, the hybrid 2S/4S solver has a better compromise between accuracy and computational efficiency (Fu et al., 1997). The default ice-cloud optics in the E3SMv2 do not include ice-cloud scattering properties in the LW. In this study, cloud optical properties, including cloud extinction coefficients, single-scattering albedo, and asymmetry factors, are based on a cloud particle shape model (Yang et al., 2018) consistent with that used for the Moderate Resolution Imaging Spectroradiometer (MODIS) Collection 6 operational cloud products (Platnick et al., 2015; 2017). Details about the LW radiative transfer solver and ice-cloud topics can be found in Kuo et al. (2020) and Chen et al. (2020).

2.3. Numerical experiment design and data analysis

The scheme described in the previous subsection has been ported to the E3SMv2. We carried out two sets of simulations: one with cloud LW scattering on (hereafter referred to as Scat), and one with that option off (hereafter referred to as noScat). The rest specifications of the two sets of

simulations are identical. By comparing the two sets of simulations, we can deduce the effects of cloud LW scattering on the simulated climate. Each set of simulations consists of three 35-year runs branching from Year 101, 151, and 251 of the piControl simulation, respectively. The mean-state differences are computed as the averaged differences between these three 35-year runs. Note that the noScat run is not the same as the standard piControl run because the default ice-cloud optics are replaced with MODIS Collection 6 ice optics, and the radiative transfer solver is swapped by the hybrid 2S/4S solver with the scattering capability. For this reason, the noScat case is also compared to the piControl case in the following section.

In addition, to compare the effect caused by ice cloud scattering to that caused by increasing greenhouse gases, another set of runs was carried out, namely noScat_4xCO2. The configuration is almost the same as the noScat case, but the CO_2 concentration is fixed at 4 times as large as that in the noScat case. We only did one 35-year run that branches from Year 101 of the piControl run, and this will be compared to the corresponding 35-year run of the noScat case to show the effect of abrupt 4xCO_2 concentration simulated by the E3SMv2 model.

3. TOA Energy Imbalance and Surface Temperature Accumulation

As no additional tuning has been done other than the scheme modification mentioned in Section 2, it is necessary to examine the time series of TOA (top-of-the-atmosphere) energy imbalance first to ensure that the model integration has reached a quasi-equilibrium state. Figure 1a shows the annual-mean time series of TOA energy imbalance, defined as the TOA net radiative flux (downward positive). The annual-mean TOA energy imbalance time series of the piControl case

has a mean of -0.003 W m^{-2} and a standard deviation of 0.24 W m^{-2} (blue lines in Figure 1a). The imbalance time series of the noScat case (black lines in Figure 1a) has a mean of -0.32 W m^{-2} and a standard deviation of 0.23 W m^{-2}. When ice-cloud LW scattering is turned on (Scat runs), the imbalance time series has a mean of -0.05 W m^{-2} with a standard deviation of 0.18 W m^{-2} (red lines in Figure 1a). Therefore, as far as TOA energy imbalance is concerned, both noScat and Scat runs only deviate from the piControl run modestly with comparable year-to-year fluctuations. Consistent with such TOA energy imbalance differences, the global-mean surface skin temperature in the Scat case is higher than that in the noScat case by ~0.37 K but very similar to the global-mean surface skin temperature in the piControl case (Figure 1b).

4. A Refined Understanding of the Temperature Response to the inclusion of LW ice cloud scattering

As shown in previous studies (Costa & Shine, 2006; Kuo et al., 2017), the inclusion of LW cloud scattering in offline radiative transfer calculations can reduce the global-mean OLR by 1.5~3 Wm^{-2}. Therefore, when cloud LW scattering is enabled, it effectively increases the instantaneous radiative forcing of the originally modeled climate system that ignores cloud LW scattering. We could expect that, to some extent, the temperature response to cloud LW scattering should resemble the temperature response to the increase of greenhouse gases, which also leads to an increase of the instantaneous radiative forcing.

4.1. Temperature response in different climate zones

Figure 2 shows the temperature profiles in different climate zones as well as their differences due

196 to the cloud LW scattering effect. Climate zones examined here are the tropics (30ºS-30ºN), the
197 mid-latitude (30-60 degrees in both hemispheres), the Arctic (60ºN-90ºN), and the Antarctic (60ºS-
198 90ºS). The global mean profiles are also plotted for reference. In addition to the annual-mean
199 differences shown in Figure 2b, Figures 2c and 2d show the seasonal-mean differences in the
200 boreal winter and summer, respectively. Globally speaking, the cloud LW scattering effect results
201 in warming through the troposphere by ~0.5 K (Figure 2b). Similar to the warming induced by the
202 increase of CO_2 (Figure S1), the warming in the tropical upper troposphere (~0.75K) is larger than
203 the tropical surface warming in all three panels, which can be explained by the fact that the
204 troposphere in the tropics is close to moist adiabatic and remains so as it warms (Manabe &
205 Wetherald, 1975; Manabe & Stouffer, 1980). The annual-mean differences in the Arctic lower
206 troposphere are about twice as much as the differences in other regions (including the global mean).
207 The near-surface warming in the Arctic, confined within the stratification layer due to small
208 turbulent heat flux (Boeke et al., 2021), can reach > 1.5 K in the winter and drop to 0.5 K or even
209 lower in the summer. Similar latitudinal patterns and seasonal dependence also appear in the zonal-
210 mean surface skin temperature (Figure 3a; also Figure S2 for spatial distribution) and surface
211 downward LW flux (Figure 3b). Like what has been shown in Chen et al. (2020), downward LW
212 flux at the surface is positively correlated with surface skin temperature ($r = 0.95$ for DJF and
213 $r = 0.69$ for JJA). Such a seasonally dependent Arctic warming pattern is also similar to the
214 pattern caused by the increase of CO_2 (Figure S3).

215 **4.2. <u>On the strong surface warming in the Arctic</u>**

Contributions to the strong warming in the Arctic, especially in boreal winter, are multifold. First, LW scattering by clouds is more effective when the gaseous absorption is weaker. More LW radiation scattered by the clouds can reach the surface without being absorbed by the atmosphere when the air temperature is low and the total column water vapor is limited (Figure 1 in Chen et al., 2020). Second, the Arctic climate feedback, including lapse rate feedback, cloud feedback, and surface albedo feedback, together can double the warming rate of the Arctic with respect to the global-mean warming rate (Stuecker et al., 2018). Third, in boreal summer, the surface temperature increase in the summer season is dampened by sea ice melting and energy storage from summer to fall/winter seasons (Boeke et al., 2021).

Similar to the approach adopted by Zhao et al. (2018) to quantitatively separate the instantaneous effect of the scattered LW flux by clouds and the indirect effect due to feedbacks, we ran an additional set of 3-year simulations branching from year 101 of the piControl run that is configured similar to the Scat case. While these runs evolve with cloud LW scattering enabled, the model outputs additional longwave radiative fluxes and longwave heating rates computed in parallel but without the cloud LW scattering effect. This case will be referred to as "Scat_offline" in the following discussion. The difference between the Scat case and the Scat_offline case is the instantaneous (or direct) radiative effect by cloud LW scattering. Over the course of three years, the differences show small seasonal variations (~1 W/m^2 for OLR and ~0.2 W/m^2 for FLDS), and the annual-mean differences change little (Figure S4). Thus, we expect that the instantaneous effect (Scat – Scat_offline) derived from such a three-year simulation can be used to represent the

instantaneous effect for the 35-year simulation. Then the indirect effect (i.e., caused by the feedbacks of the climate system) can thus be obtained from the difference between the total effect (Scat – noScat) and the instantaneous effect (Scat – Scat_offline).

The decomposition of the changes in OLR and FLDS in such a way is summarized in Figures 4a and 4b, respectively. OLR is reduced globally by 1.13 W/m^2 on average due to the direct cloud LW scattering effect. This is lower than the suggested values from previous studies (1.5~3.0 W/m^2) (Costa & Shine, 2006; Kuo et al., 2017), which is to some extent due to the neglect of liquid cloud LW scattering. The largest decrease occurs in the tropics by 2 W/m^2, while the smallest decrease occurs in the polar region and the subtropical region (<1 W/m^2). The large OLR reduction in the tropics is consistent with Kuo et al. (2017) and Costa & Shine (2006), where they found a maximal decrease over the tropical convective zone. This is due to small cloud particles (Figure S5), a large amount of ice cloud in the tropical convective core, and the large temperature contrast between the cloud top and surface. Both atmosphere and surface warm to increase the OLR so that net LW flux at TOA decreases towards 0 (a small difference of 0.04 W/m^2). The direct FLDS increase due to the scattered LW flux by ice clouds is more than one order of magnitude smaller compared to the feedbacks (0.08 W/m^2 versus 2.19 W/m^2 globally). The little impact on the downward LW flux at the surface due to direct cloud LW scattering is consistent with the finding in Zhao et al. (2018). The FLDS increase due to feedback is more prominent in the Arctic by up to 5 W/m^2 compared to ~2 W/m^2 in the tropics, while the increase due to direct cloud LW scattering itself has little latitudinal variation. This suggests that the large increase of FLDS in the Arctic is dominantly

caused by the feedback process, where the warmer atmosphere emits more LW radiation to the surface. Because of the positive correlation of FLDS and TS, it can be inferred that strong surface warming in the Arctic is dominantly caused by the Arctic amplification resulting from the additional TOA radiative forcing due to cloud LW scattering.

In a nutshell, including the ice cloud LW scattering effect induces a small warming effect globally. The latitudinal structure and seasonal dependence of the warming are, to a large extent, similar to those induced by radiative forcing due to the increase of CO_2. Arctic amplification due to positive feedback in the Arctic is the primary contributor to the strong warming as well as more downward LW flux at the surface. In response to the OLR reduction and the consequent temperature increase throughout the globe, cloud fraction and properties will also be modified. We will focus on the tropical cloud changes in the following section, as these changes are also characteristic in response to the increase of CO_2 (Sherwood et al., 2020).

5. Consequent Cloud Changes in the Tropics

5.1. Mid-Tropospheric Cloud Ice Reduction

To quantitatively study the cloud phase transition in the simulated climate, we define a unitless variable R to represent the percentage of ice within clouds:

$$R = \frac{r_{ice}}{r_{ice} + r_{liquid}},$$

where r_{ice} is the in-cloud ice mixing ratio and r_{liquid} is the in-cloud liquid mixing ratio. Both quantities have a unit of kg/kg. The valid range of the ratio is from 0 to 1, and it will increase to 1

when a cloud is dominantly in the ice phase.

Figure 5a shows the global and regional vertical profiles of R. As the altitude increases, ice particles gradually dominate the clouds. There is a peak in R at ~500 hPa in the tropics, which mainly comes from the convective in-cloud water. Figure 5b-d shows the change of R due to the cloud LW scattering effect in different seasons. The strongest decrease in ice partition, up to 8%, occurs in the tropical mid-troposphere. The spatial distribution of R at 575 hPa is shown in Figure 6, indicating that the decrease in ice cloud amount occurs across the tropical region, especially over the Indian ocean. Meanwhile, noticeable decreases in ice cloud amount can also be seen at 450 hPa in the summer Arctic, 600 hPa in the winter Arctic, and 300 hPa in the tropics.

Figure 7 shows the correlation between the ice cloud amount and the temperature at 575 hPa, where each point in the upper-panel plot represents the 35-year average cloud ice ratio R and air temperature for a grid box in the tropics. The bottom panel is a histogram of the air temperature in both Scat and noScat cases. The cloud ice ratio negatively correlates with the air temperature ($r \approx -0.5$). When the mean temperature increases by ~0.5 K, the cloud ice ratio drops by about 10%. Note that the layer temperature at 575 hPa is close to the freezing point of pure water (273.15 K, purple dashed line). A slight perturbation in the temperature profile can result in a considerable cloud phase transition at this pressure level.

5.2. High Cloud Lift and Anvil Cloud Reduction

As defined in the E3SMv2 model, we regard a cloud with top pressure > 700 hPa as a low cloud

294 and a cloud with top pressure < 400 hPa as a high cloud. Figure 8 shows the spatial distribution of
295 35-year mean high cloud fraction and low cloud fraction, as well as the changes due to the cloud
296 LW scattering effect. Commonly known features such as ITCZ (Inter-Tropical Convergence Zone)
297 and SPCZ (Southern-Pacific Convergence Zone) are well captured in Figure 8a. The differences
298 due to cloud LW scattering (Figure 8b) show a statistically significant ($p < 0.01$) reduction of high
299 cloud fraction by ~0.03 over the SPCZ clouds. Other statistically significant but relatively smaller
300 decreases are seen in the tropical Atlantic Ocean and the Indian Ocean. These high cloud responses
301 are analogous to the response due to the increase of CO_2 predicted by the E3SMv2 model, except
302 that the strong high cloud fraction increase over the eastern tropical Pacific driven by the increase
303 of CO_2 is missing in response to cloud LW scattering (Figure 8c).

304 Figure 9 focuses on the changes of vertically-resolved cloud fraction to show high-cloud fraction
305 changes in detail. The most noticeable change is an increase of cloud fraction by up to 0.02
306 (50%~100% relative change) at 100 hPa, especially over the western Pacific warm pool region.
307 Other two deep convective regions along ITCZ, i.e., over tropical Africa and Amazon, also show
308 an increase of cloud fraction, but not as larger as the warm pool region. Note that the overall high-
309 cloud fraction differences over such deep convective core regions are close to zero (Figure 8b).
310 Therefore, such an increase in cloud fraction at 100 hPa must be accompanied by a decrease in
311 cloud fraction at levels below it. This corresponds to the cloud fraction reduction below at 250 hPa.
312 Moreover, the decrease of cloud fraction at 250 hPa is more extensive than the increase of cloud
313 fraction at 100 hPa, with noticeable decreases around the deep convective regions (near the 180º

longitude line), i.e., a reduction of anvil clouds. The 100-hPa cloud fraction increase over the deep convective regions is consistent with the lift of high clouds, i.e., high-cloud altitude feedback, usually referred to as fixed anvil temperature (FAT) or proportionately higher anvil temperature (PHAT) hypothesis (Hartmann & Larson, 2002; Zelinka & Hartmann, 2010, 2011; Yoshimori et al., 2020). The 250-hPa cloud fraction decrease over extensive tropical regions is more related to the high-cloud amount feedback (Bony et al., 2016; Mauritsen & Stevens, 2015).

5.3. Stratiform Low Cloud Increase over Southern Tropical Ocean

Figure 8d and 8e show the low cloud fraction without cloud LW scattering and the difference caused by cloud LW scattering. Low clouds in the tropical ocean concentrate in the subtropical eastern boundary of each ocean basin, i.e., the subsidence branches of the longitudinal circulations. Figure 8e shows three regions of low cloud increase in the southern tropical oceans. An increase of low cloud fraction by ~0.04 (5~10% relatively) is seen over the southeastern tropical Pacific and southern subtropical Atlantic, both regions known for the frequent occurrence of stratiform low clouds. An increase of low cloud coverage is also seen over the Indian Ocean, but not as large as the above two regions. These low cloud increases are analogous to the response due to the increase of CO_2 predicted by the E3SMv2 model except the magnitude and significance (Figure 8f).

The increasing amount of stratiform low clouds in these regions can be explained using estimated inversion strength (EIS) and surface temperature (T_S) changes, where EIS is similar to lower tropospheric stability (LTS) that estimates the strength of the PBL inversion depending only upon

700 hPa temperature and surface temperature (Wood & Bretherton, 2006). Figure 10 shows the monthly mean low cloud fraction change binned by the EIS and T_S changes for the aforementioned three tropical oceanic regions. An increase in low cloud fraction (bluish color) coincides with a positive change of EIS and a negative change in surface temperature (i.e., the second quadrant of each panel), and vice versa. The color gradient that is almost along the y-axis in figure 10 suggests that the simulated low cloud fraction changes are more sensitive to the EIS change than the T_S change. It is confirmed that, compared to the noScat simulations, the increasing amount of stratiform low clouds in these regions in the Scat simulations is related to stronger boundary layer inversion and cooler surface (McCoy et al., 2017; Qu et al., 2014; Wood & Bretherton, 2006). Averagely speaking, over these regions, the long-term mean of EIS increases by a small amount of 0.5 K, and the long-term mean change in T_S is negligible. This implies that the free troposphere warms more than the boundary layer. As a result, stratiform low cloud coverage increases when the ice cloud LW scattering effect is included, for the effect of LW scattering on modifying lower tropospheric and surface temperatures.

The aforementioned cloud property changes in the tropical region due to the cloud LW scattering effect are analogous to how the E3SMv2 model responds to radiative forcings from increasing well-mixed greenhouse gases like CO_2 (Figure 8c and 8f; Figures S6 & S7). Note that these cloud changes may be specific to the E3SMv2 model. Especially, the low cloud response due to cloud LW scattering may be different in other models due to the large intermodal spread in tropical marine low cloud feedback (Klein et al., 2017). Future studies are warranted to include cloud LW

354 scattering in other climate models.

355 6. Conclusions

356 We modified the E3SM version 2, a fully-coupled climate model, to include the ice cloud LW
357 scattering effect, a physical process omitted by most climate models. Based on the modified model,
358 we ran two sets of simulations, one with and the other without cloud LW scattering, to study the
359 impact of cloud LW scattering on the simulated climate system. Figure 11 summarizes the radiative
360 and temperature responses to the inclusion of cloud LW scattering. The instantaneous radiative
361 effect due to cloud LW scattering reduces the OLR across all latitudes. The strongest OLR
362 reduction occurs in the tropics. Most scattered fluxes are absorbed in the atmosphere, as the
363 instantaneous increase of FLDS is negligible compared to the OLR reduction. The reduction of
364 OLR due to the direct cloud LW scattering effect is compensated by the warming atmosphere and
365 surface through feedback processes. Consequently, the global-mean climate warms by 0.5 K, and
366 the Arctic warms at least twice as fast as the global mean, especially in boreal winter. The majority
367 of the total FLDS increase, as well as the highly correlated surface temperature increase, is
368 primarily due to the feedback processes. Tropical cloud changes include reduced ice cloud
369 presence in the middle troposphere, elevated deep convective clouds, reduced anvil cloud coverage,
370 and increased stratiform low cloud coverage. Most responses seen here are similar to those
371 responses caused by warming due to well-mixed greenhouse gases in the same E3SM v2 model.
372 For a climate model without cloud LW scattering, the inclusion of such an effect will cause
373 discernible changes in the mean-state climate through the entire troposphere over the globe, as the

374 OLR reduction directly caused by the cloud LW scattering effect (~1.13 W m^{-2} in global-mean
375 OLR) triggers climate feedbacks.

376 This study deepens and refines our understanding of the cloud LW scattering effect. The
377 explanation in Chen et al. (2020) for the simulated responses in the polar region overlooked the
378 global connections and changes in the tropics caused by cloud LW scattering. Moreover, the fully-
379 coupled model used here can better account for the complex atmosphere-ocean interactions than
380 slab-ocean or prescribed-SST models. Due to the highly sensitive nature of the polar climate, our
381 study emphasizes the importance of including the cloud LW scattering effect in climate models for
382 accurately simulating the polar climate. Although our study suggests that the cloud LW scattering
383 effect acts like an additional positive term in LW cloud forcing, it is expected that the inclusion of
384 cloud LW scattering physics can also affect the actual LW cloud feedback in the case of warming
385 induced by increasing greenhouse gases. Comparing the climate sensitivity under the $4xCO_2$
386 scenario with or without the cloud LW scattering effect is one of our follow-up studies to
387 understand the impact of such an effect on the simulated climate changes by the same model.

388 The modified model includes another piece of physics that is often neglected in climate modeling
389 studies. Compared to the original E3SMv2 model, the present modifications only cost 10%
390 additional computational time. Note that our results apply to a specific E3SM model with unique
391 model physics and tuning. But it is straightforward to apply the modifications to other climate
392 models as well. Because of the 3D nature of scattering, it would be also a meaningful study to
393 examine the cloud LW scattering effect in the context of 3D radiative transfer (e.g., Kablick et al.,

2011), especially for high-spatial-resolution global simulations such as those global storm-resolving models with a spatial resolution as high as 3~7 km. Future climate feedback studies that used such climate models with improved physics can potentially reduce uncertainties in radiative transfer and yield a more robust feedback estimation.

Acknowledgment

This material is based upon work supported by the U.S. Department of Energy, Office of Science, Office of Biological and Environmental Research, Climate and Environmental Science Division under Awards DE-SC0019278 and DE-SC0022117 to the University of Michigan with a subcontract to Texas A&M. YHC performed relevant work for this project entirely during his stay at the University of Michigan. We also thank Dr. Xianwen Jing for his contribution to code development during his postdoctoral stay at the University of Michigan.

Data Availability Statement

The source code of the original E3SM version 2 can be found in the official GitHub repository (https://github.com/E3SM-Project/E3SM). Our modifications are based on the v2.0.0 tag (https://github.com/E3SM-Project/E3SM/tree/v2.0.0) of this repository. The source code of our modified model can be found on GitHub (https://github.com/cxfan1997/E3SM). The noScat run can be reproduced using the cxfan/v2.LR.piControl.0101.UMRad.CTRL branch (https://github.com/cxfan1997/E3SM/tree/cxfan/v2.LR.piControl.0101.UMRad.CTRL), and the Scat run using the cxfan/v2.LR.piControl.0101.UMRad.Scat branch. Model outputs were

413 processed using netCDF Operator (NCO) and xarray (Hoyer & Hamman, 2017).

414 References

415 Boeke, R. C., Taylor, P. C., & Sejas, S. A. (2021). On the Nature of the Arctic's Positive Lapse-
416 Rate Feedback. *Geophysical Research Letters*, *48*(1). https://doi.org/10.1029/2020gl091109

417 Bony, S., Stevens, B., Coppin, D., Becker, T., Reed, K. A., Voigt, A., & Medeiros, B. (2016).
418 Thermodynamic control of anvil cloud amount. *Proceedings of the National Academy of*
419 *Sciences*, *113*(32), 8927–8932. https://doi.org/10.1073/pnas.1601472113

420 Chen, Y., Huang, X., Yang, P., Kuo, C., & Chen, X. (2020). Seasonal Dependent Impact of Ice
421 Cloud Longwave Scattering on the Polar Climate. *Geophysical Research Letters*, *47*(23).
422 https://doi.org/10.1029/2020gl090534

423 Chou, M.-D., Lee, K.-T., Tsay, S.-C., & Fu, Q. (1999). Parameterization for Cloud Longwave
424 Scattering for Use in Atmospheric Models. *Journal of Climate*, *12*(1), 159–169.
425 https://doi.org/10.1175/1520-0442(1999)012<0159:pfclsf>2.0.co;2

426 Costa, S. M. S., & Shine, K. P. (2006). An estimate of the global impact of multiple scattering by
427 clouds on outgoing long-wave radiation. *Quarterly Journal of the Royal Meteorological*
428 *Society*, *132*(616), 885–895. https://doi.org/10.1256/qj.05.169

Eyring, V., Bony, S., Meehl, G. A., Senior, C. A., Stevens, B., Stouffer, R. J., & Taylor, K. E. (2016). Overview of the Coupled Model Intercomparison Project Phase 6 (CMIP6) experimental design and organization. *Geoscientific Model Development*, *9*(5), 1937–1958. https://doi.org/10.5194/gmd-9-1937-2016

Fu, Q., Liou, K. N., Cribb, M. C., Charlock, T. P., & Grossman, A. (1997). Multiple Scattering Parameterization in Thermal Infrared Radiative Transfer. *Journal of the Atmospheric Sciences*, *54*(24), 2799–2812. https://doi.org/10.1175/1520-0469(1997)054<2799:mspiti>2.0.co;2

Golaz, J.-C., Caldwell, P. M., Van Roekel, L. P., Petersen, M. R., Tang, Q., Wolfe, J. D., et al. (2019). The DOE E3SM coupled model version 1: Overview and evaluation at standard resolution. *Journal of Advances in Modeling Earth Systems, 11*, 2089–2129. https://doi.org/10.1029/2018MS001603

Golaz, J.-C., Van Roekel, L. P., Zheng, X., Roberts, A. F., Wolfe, J. D., Lin, W., et al. (2022). The DOE E3SM Model Version 2: Overview of the physical model and initial model evaluation. *Journal of Advances in Modeling Earth Systems, 14*, e2022MS003156. https://doi.org/10.1029/2022MS003156

Hartmann, D. L., & Short, D. A. (1980). On the Use of Earth Radiation Budget Statistics for Studies of Clouds and Climate. *Journal of the Atmospheric Sciences*, *37*(6), 1233–1250. https://doi.org/10.1175/1520-0469(1980)037<1233:otuoer>2.0.co;2

Hartmann, D. L. & Larson, K. (2002). An important constraint on tropical cloud - climate feedback. *Geophysical Research Letters, 29*, 1951. https://doi.org/10.1029/2002GL015835

Holland, M. M., & Bitz, C. M. (2003). Polar amplification of climate change in coupled models. *Climate Dynamics*, *21*, 221–232. https://doi.org/10.1007/s00382-003-0332-6

Hoyer, S. & Hamman, J., (2017). xarray: N-D labeled Arrays and Datasets in Python. *Journal of Open Research Software, 5*(1), 10. https://doi.org/10.5334/jors.148

Jin, Z., Zhang, Y., Genio, A. D., Schmidt, G., & Kelley, M. (2019). Cloud scattering impact on thermal radiative transfer and global longwave radiation. *Journal of Quantitative Spectroscopy and Radiative Transfer*, *239*, 106669. https://doi.org/10.1016/j.jqsrt.2019.106669

Joseph, E., & Min, Q. (2003). Assessment of multiple scattering and horizontal inhomogeneity in IR radiative transfer calculations of observed thin cirrus clouds. *Journal of Geophysical Research: Atmospheres*, *108*, 4380. https://doi.org/10.1029/2002jd002831

Kablick, G. P., Ellingson, R. G., Takara, E. E., & Gu, J. (2011). Longwave 3D Benchmarks for Inhomogeneous Clouds and Comparisons with Approximate Methods. *Journal of Climate 24*, 2192–2205. https://doi.org/10.1175/2010jcli3752.1

Klein, S.A., Hall, A., Norris, J.R., & Pincus, R. (2017). Low-Cloud Feedbacks from Cloud-Controlling Factors: A Review. *Surveys in Geophysics, 38*, 1307–1329. https://doi.org/10.1007/s10712-017-9433-3

Kuo, C., Yang, P., Huang, X., Feldman, D., Flanner, M., Kuo, C., & Mlawer, E. J. (2017). Impact of Multiple Scattering on Longwave Radiative Transfer Involving Clouds. *Journal of Advances in Modeling Earth Systems*, *9*(8), 3082–3098. https://doi.org/10.1002/2017ms001117

Kuo, C., Yang, P., Huang, X., Chen, Y.., & Liu, G. (2020). Assessing the accuracy and efficiency of longwave radiative transfer models involving scattering effect with cloud optical property parameterizations. *Journal of Quantitative Spectroscopy and Radiative Transfer*, *240*, 106683. https://doi.org/10.1016/j.jqsrt.2019.106683

Li, J., & Fu, Q. (2000). Absorption Approximation with Scattering Effect for Infrared Radiation. *Journal of the Atmospheric Sciences*, *57*(17), 2905–2914. https://doi.org/10.1175/1520-0469(2000)057<2905:aawsef>2.0.co;2

Manabe, S., & Wetherald, R. T. (1975). The Effects of Doubling the CO2 Concentration on the climate of a General Circulation Model. *Journal of the Atmospheric Sciences, 32*(1), 3–15. https://doi.org/10.1175/1520-0469(1975)032<0003:teodtc>2.0.co;2

Manabe, S., & Stouffer, R. J. (1980). Sensitivity of a global climate model to an increase of CO2 concentration in the atmosphere. *Journal of Geophysical Research: Oceans, 85*(C10), 5529–5554. https://doi.org/10.1029/jc085ic10p05529

Mauritsen, T., & Stevens, B. (2015). Missing iris effect as a possible cause of muted hydrological change and high climate sensitivity in models. *Nature Geoscience*, *8*(5), 346–351. https://doi.org/10.1038/ngeo2414

McCoy, D. T., Eastman, R., Hartmann, D. L., & Wood, R. (2017). The Change in Low Cloud Cover in a Warmed Climate Inferred from AIRS, MODIS, and ERA-Interim. *Journal of Climate*, *30*(10), 3609–3620. https://doi.org/10.1175/jcli-d-15-0734.1

Platnick, S., Meyer, K. G., King, M. D., Wind, G., Amarasinghe, N., Marchant, B., et al. (2015). *MODIS cloud optical properties: User guide for the collection 6 level-2 MOD06/MYD06 product and associated level-3 datasets, version 1.0*. Retrieved from http://modis-atmos.gsfc.nasa.gov/_docs/C6MOD06OPUserGuide.pdf

Platnick, S., Meyer, K. G., King, M. D., Wind, G., Amarasinghe, N., Marchant, B., et al. (2017). The MODIS Cloud Optical and Microphysical Products: Collection 6 Updates and Examples from Terra and Aqua. *IEEE Transactions on Geoscience and Remote Sensing*, *55*(1), 502–525. https://doi.org/10.1109/tgrs.2016.2610522

Qu, X., Hall, A., Klein, S. A., & Caldwell, P. M. (2014). On the spread of changes in marine low cloud cover in climate model simulations of the 21st century. *Climate Dynamics*, *42*, 2603–2626. https://doi.org/10.1007/s00382-013-1945-z

Ritter, B., & Geleyn, J.-F. (1992). A Comprehensive Radiation Scheme for Numerical Weather Prediction Models with Potential Applications in Climate Simulations. *Monthly Weather Review*, *120*(2), 303–325. https://doi.org/10.1175/1520-0493(1992)120<0303:acrsfn>2.0.co;2

Schmidt, G. A., Ruedy, R., Hansen, J. E., Aleinov, I., Bell, N., Bauer, M., et al. (2006). Present-Day Atmospheric Simulations Using GISS ModelE: Comparison to In Situ, Satellite, and Reanalysis Data. *Journal of Climate*, *19*(2), 153–192. https://doi.org/10.1175/jcli3612.1

Sherwood, S. C., Webb, M. J., Annan, J. D., Armour, K. C., Forster, P. M., Hargreaves, J. C., et al. (2020). An Assessment of Earth's Climate Sensitivity Using Multiple Lines of Evidence. *Reviews of Geophysics*, *58*(4), e2019RG000678. https://doi.org/10.1029/2019rg000678

Stephens, G. L. (1980). Radiative Properties of Cirrus Clouds in the Infrared Region. *Journal of the Atmospheric Sciences*, *37*(2), 435–446. https://doi.org/10.1175/1520-0469(1980)037<0435:rpocci>2.0.co;2

Stephens, G. L. (2005). Cloud Feedbacks in the Climate System: A Critical Review. *Journal of Climate, 18*(2), 237–273. https://doi.org/10.1175/jcli-3243.1

515 Stuecker, M. F., Bitz, C. M., Armour, K. C., Proistosescu, C., Kang, S. M., Xie, S.-P., et al.
516 (2018). Polar amplification dominated by local forcing and feedbacks. *Nature Climate*
517 *Change*, *8*(12), 1076–1081. https://doi.org/10.1038/s41558-018-0339-y

518 Wood, R., & Bretherton, C. S. (2006). On the Relationship between Stratiform Low Cloud Cover
519 and Lower-Tropospheric Stability. *Journal of Climate*, *19*(24), 6425–6432.
520 https://doi.org/10.1175/jcli3988.1

521 Yang, P., S. Hioki, M. Saito, C.-P. Kuo, B. A. Baum, K.-N. Liou, 2018: A review of ice cloud
522 optical property models for satellite remote sensing, *Atmosphere, 9*, 499.
523 https://doi.org/10.3390/atmos9120499

524 Yoshimori, M., Lambert, F. H., Webb, M. J. & Andrews, T. (2020). Fixed anvil temperature
525 feedback - positive, zero or negative? *Journal of Climate, 33*, 2719–2739.
526 https://doi.org/10.1175/JCLI-D-19-0108.1

527 Zelinka, M. D., & Hartmann, D. L. (2010). Why is longwave cloud feedback positive? *Journal*
528 *of Geophysical Research: Atmospheres*, *115*, D16117. https://doi.org/10.1029/2010jd013817

529 Zelinka, M. D., & Hartmann, D. L. (2011). The observed sensitivity of high clouds to mean
530 surface temperature anomalies in the tropics. *Journal of Geophysical Research: Atmospheres*,
531 *116*, D23103. https://doi.org/10.1029/2011jd016459

Zhao, W., Peng, Y., Wang, B., & Li, J. (2018). Cloud Longwave Scattering Effect and Its Impact on Climate Simulation. *Atmosphere*, *9*(4), 153. https://doi.org/10.3390/atmos9040153

Figures

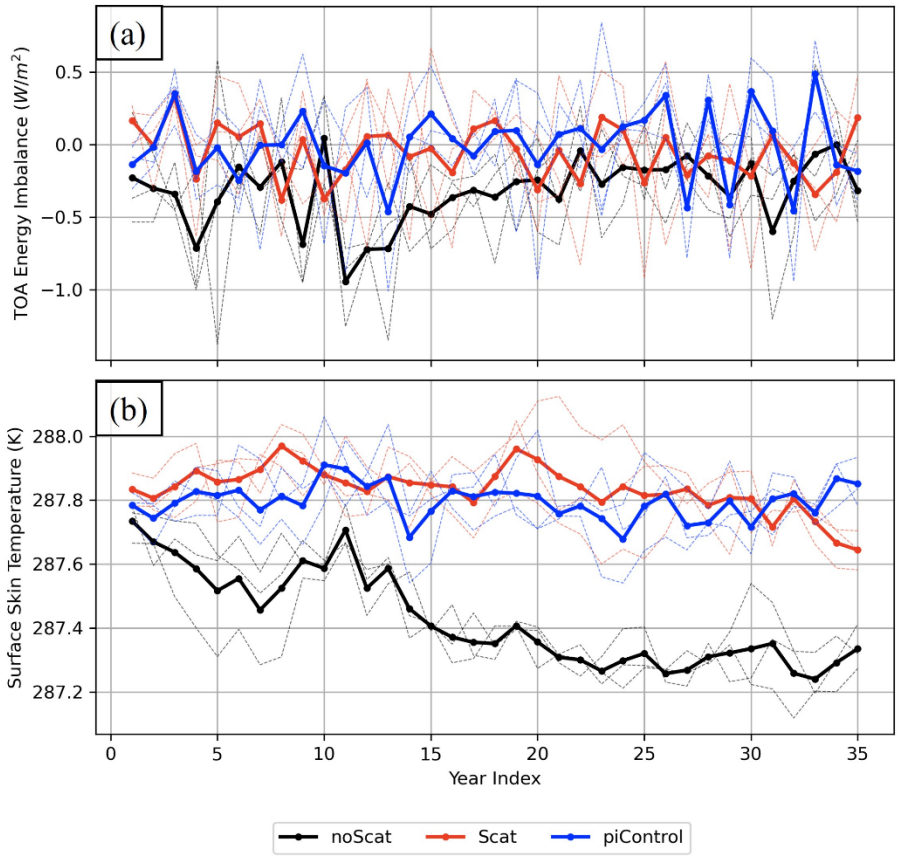

Figure 1. Annual-mean time series of (a) global mean energy imbalance at the top of the atmosphere (TOA), defined as net downward flux; and (b) global mean surface skin temperature. The Scat and noScat cases are shown in red and black, respectively, whereas the piControl case is in blue. Solid lines are for the average of three 35-year segments, whereas dashed lines are for the individual segments.

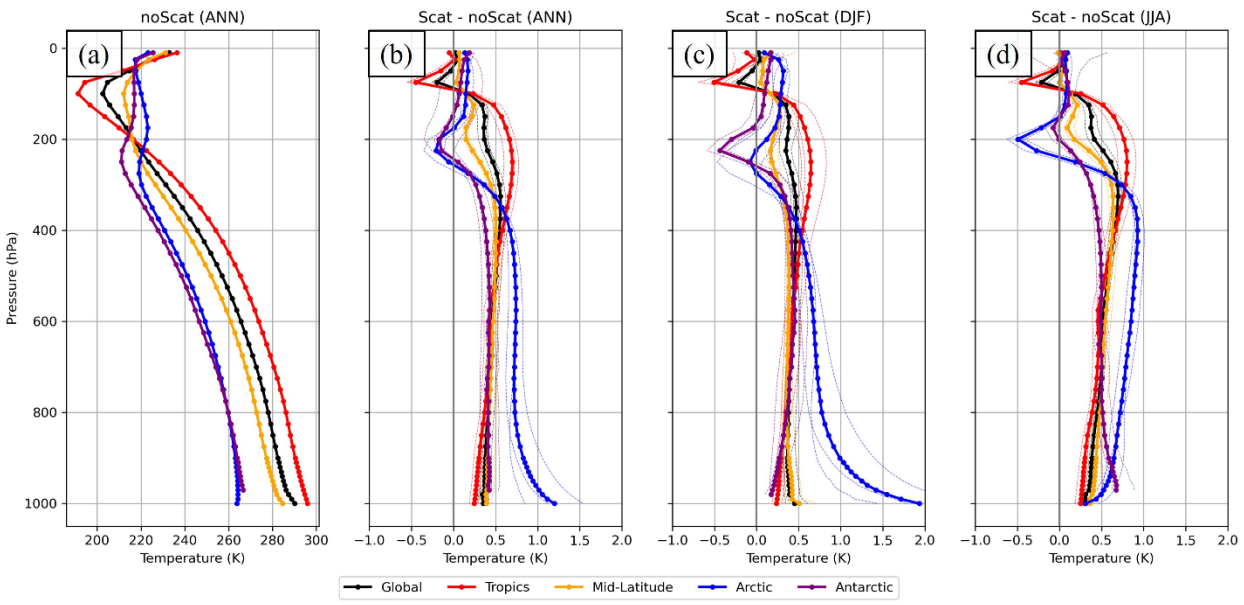

Figure 2. Differences in the atmospheric temperature profiles between the Scat and the noScat cases averaged over different climate zones and different seasons. (a) Temperature profile of the noScat case. (b) 35-year annual-mean temperature profile difference. (c) The 35-year mean difference in DJF. (d) The difference in JJA. Different colors represent different climate zones as labeled, i.e., tropics (30ºS-30ºN), mid-latitude (30ºS-60ºS and 30ºN-60ºN), Arctic (60ºN-90ºN), and Antarctic (60ºS-90ºS). The solid lines with dots are the average over three 35-year segments. Each dashed line represents an individual 35-year averaged difference.

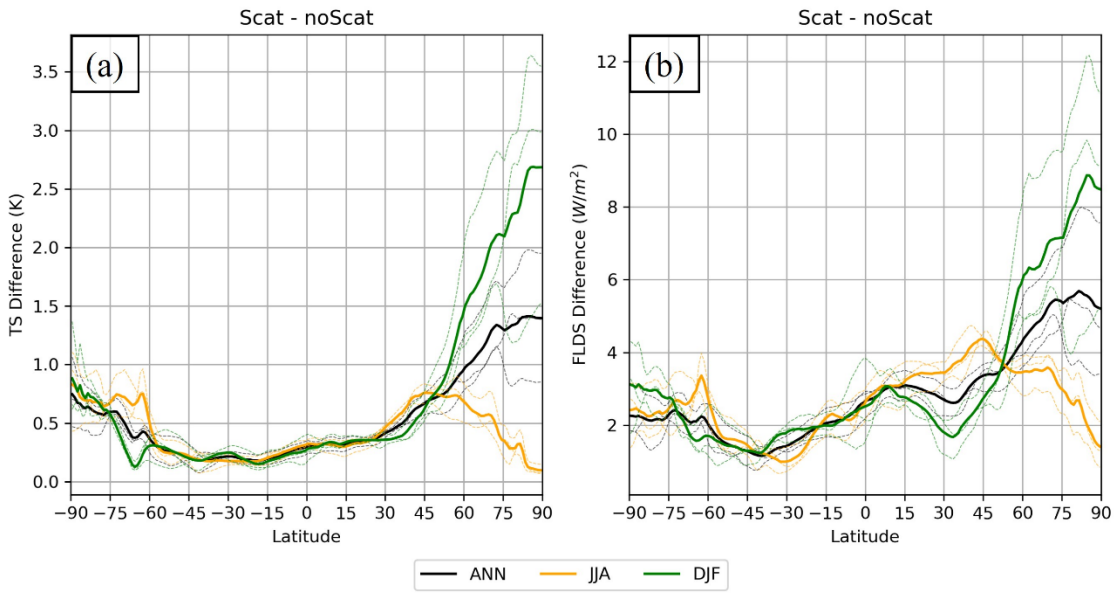

552

553 **Figure 3.** (a) 35-year zonal-mean surface skin temperature difference between the Scat and the
554 noScat cases. Black lines show the annual mean difference, while yellow and green lines show the
555 differences for JJA and DJF, respectively. Dashed lines of different colors show the changes
556 averaged over each individual 35-year segment. (b) Similar to (a), but for differences in the surface
557 downward LW fluxes.

558

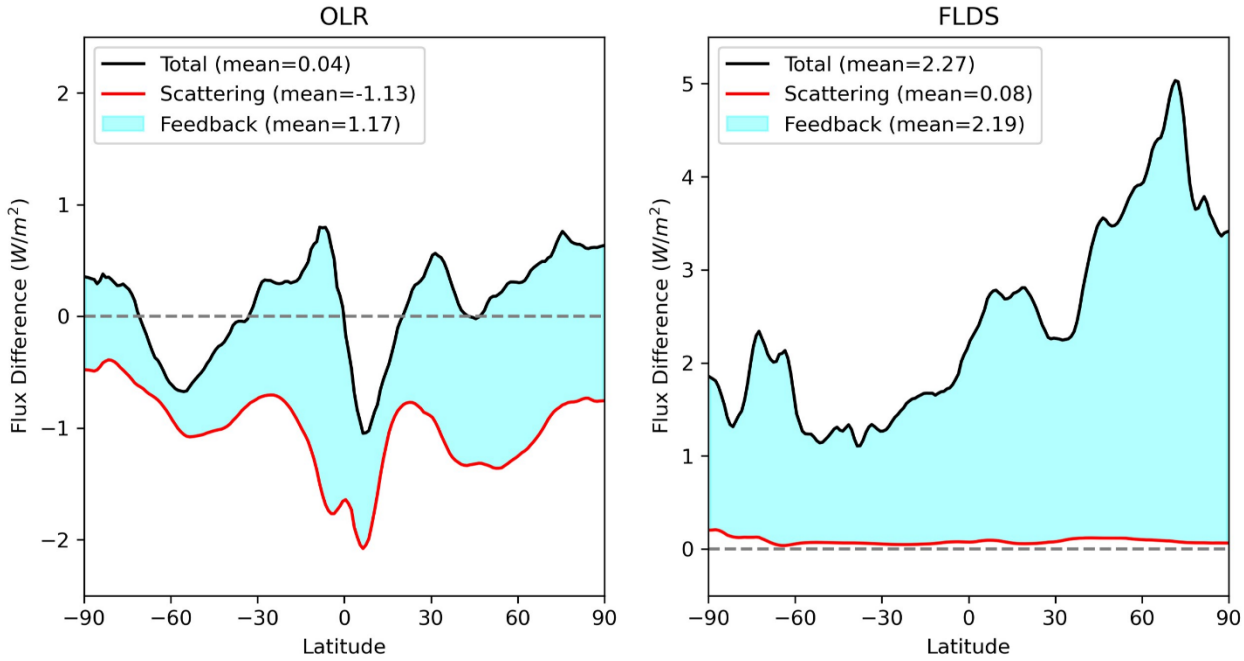

559

560 **Figure 4.** (a) Decomposition of the direct radiative effect due to direct cloud LW scattering (red
561 line) and the climate system feedbacks (blue shade) for the difference in outgoing longwave
562 radiation (OLR) between the Scat and noScat cases; (b) Same as (a) but for the difference in surface
563 downward longwave flux. The black line represents the total differences. The global mean change
564 of each component is noted in the legend.

565

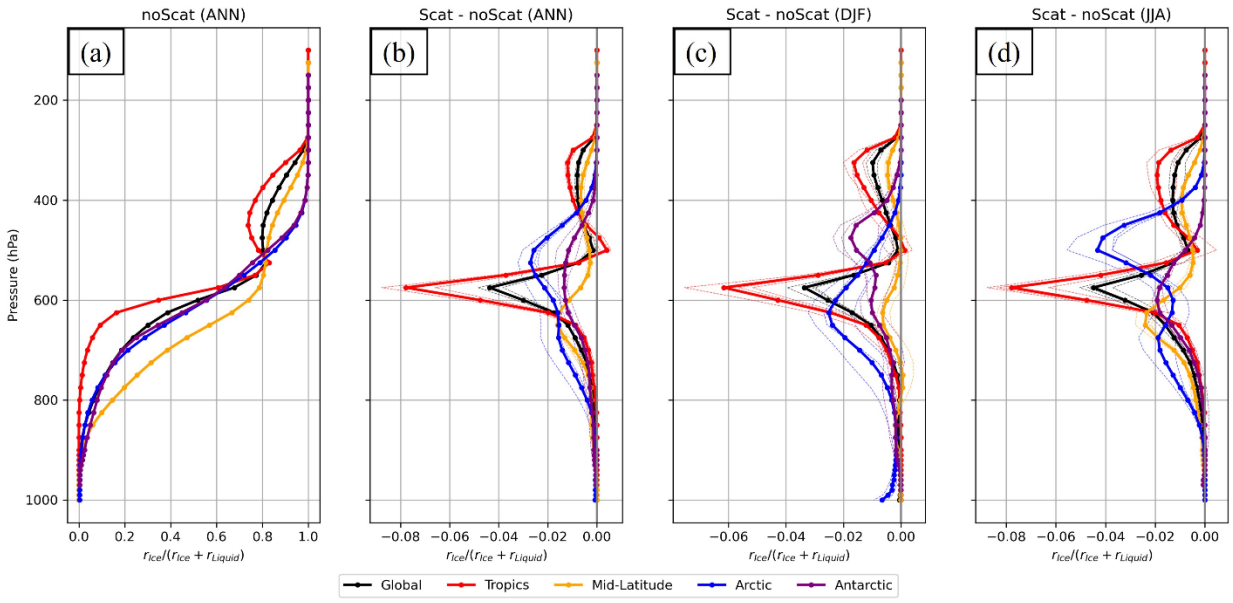

566

567 **Figure 5.** Similar to Figure 2, but for the ratio of in-cloud ice mixing ratio versus in-cloud

568 condensed water mixing ratio. The definition of the symbols is in the main text.

569

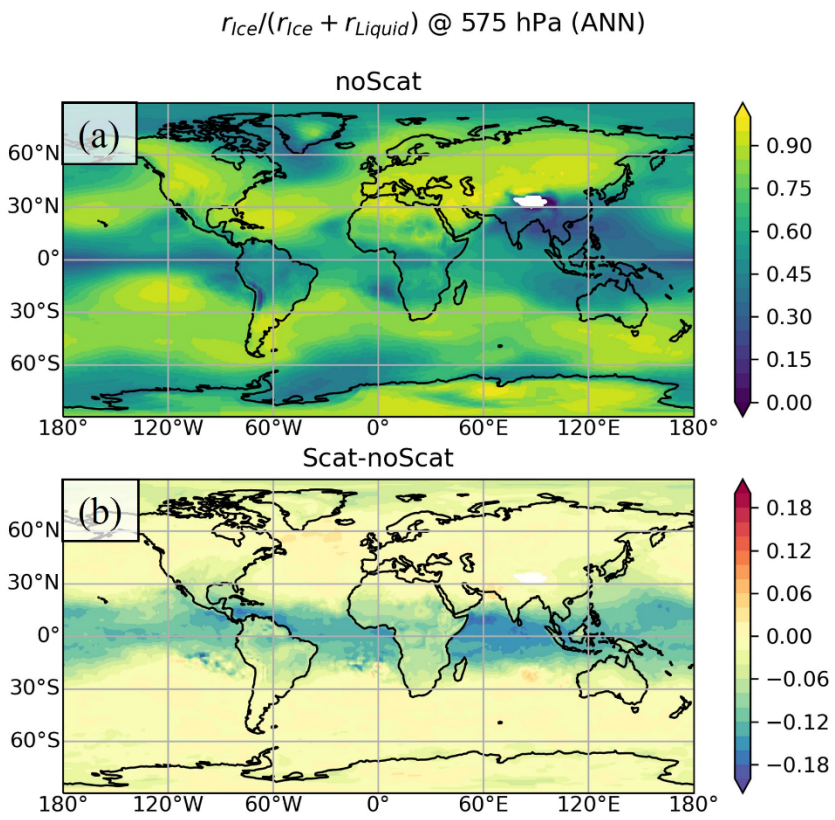

570

571 **Figure 6.** (a) Global map of the ratio of in-cloud ice mixing ratio versus in-cloud condensed water

572 mixing ratio in the noScat run. (b) The difference of the quantity between the Scat run and the

573 noScat run.

574

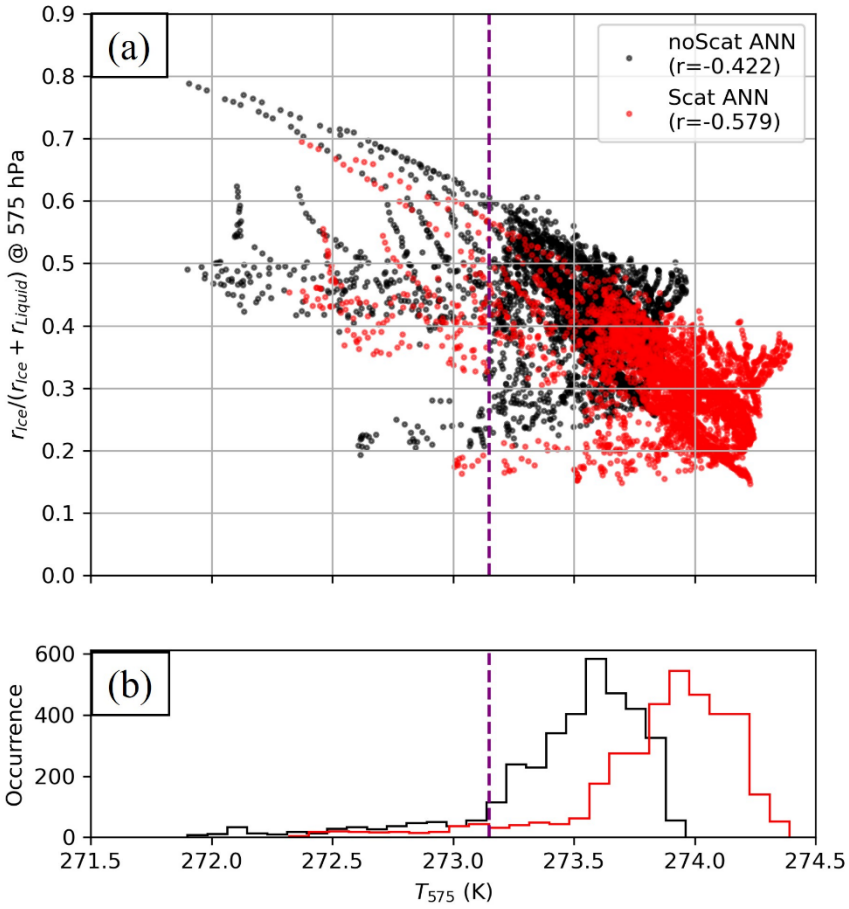

575

576 **Figure 7.** (a) Scatterplot of the ratio of in-cloud ice mixing ratio versus in-cloud condensed water
577 mixing ratio with respect to 575 hPa air temperature for all the grids within the inner tropics (20ºS-
578 20ºN). The black dots are 35-year averages from the noScat run, while the red dots are from the
579 Scat run. The correlation coefficient for each set of samples is included in the legend. (b)
580 Histogram of 575-hPa temperature in the noScat run (black) and the Scat run (red). The purple
581 dashed lines in both panels indicate the water freezing point, 273.15 K.

582

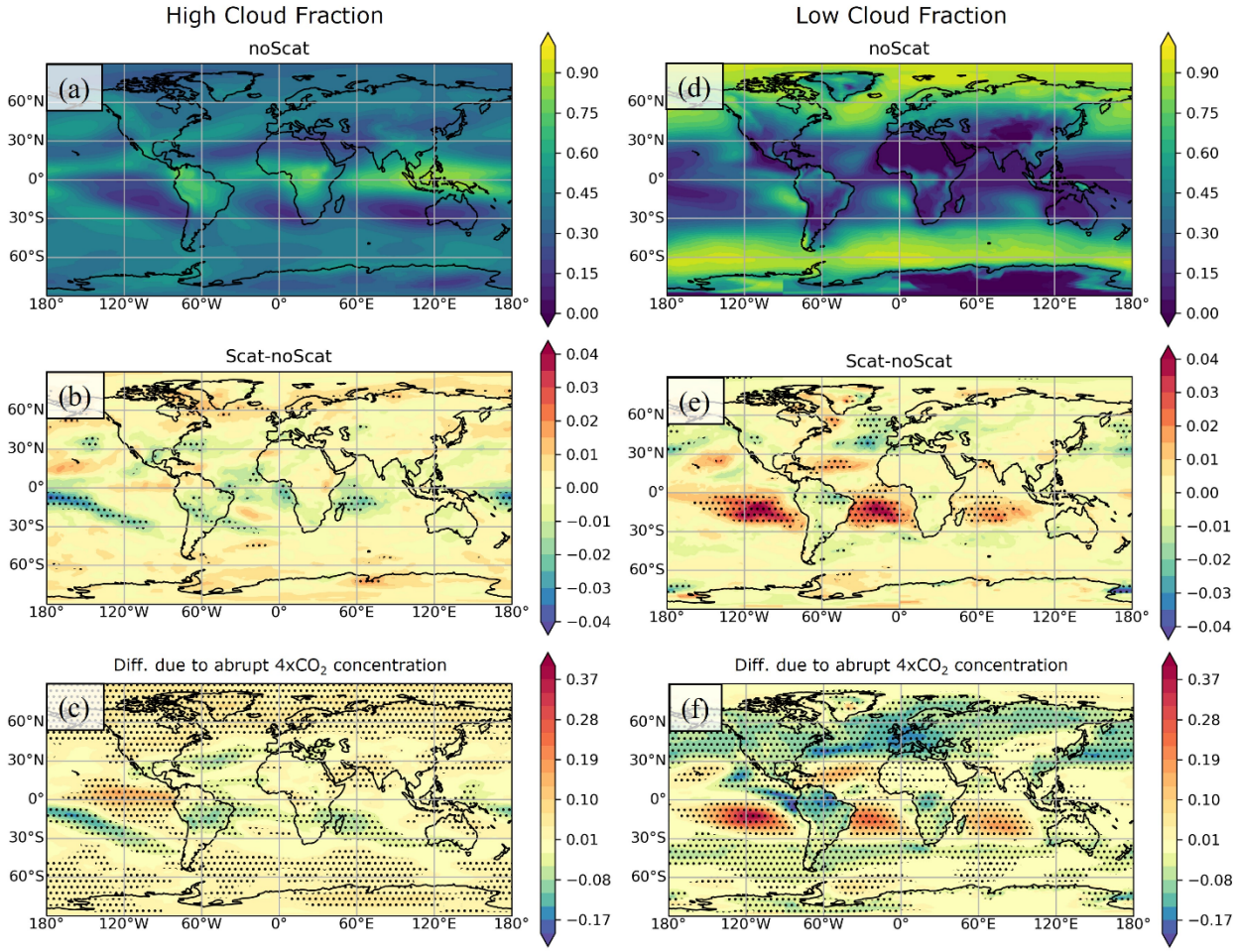

583

584 **Figure 8.** Filled contour maps of (a) high cloud fraction without cloud LW scattering (i.e., the
585 climatology of noScat run); (b) high cloud fraction change due to cloud LW scattering effect (i.e.,
586 Scat – noScat); (c) high cloud fraction change due to the abrupt increase of CO_2 to 4 times as large;
587 (d) low cloud fraction without cloud LW scattering; (e) low cloud fraction change due to cloud
588 LW scattering; and (f) low cloud fraction change due to the abrupt increase of CO_2 to 4 times as
589 large;. Black dots in panel (b-c) and (e-f) denotes statistically significant differences with a p-
590 value < 0.01. Panels (a-b) and (d-e) are 3×35-year mean, while panels (c) and (f) use 35-year
591 mean.

592

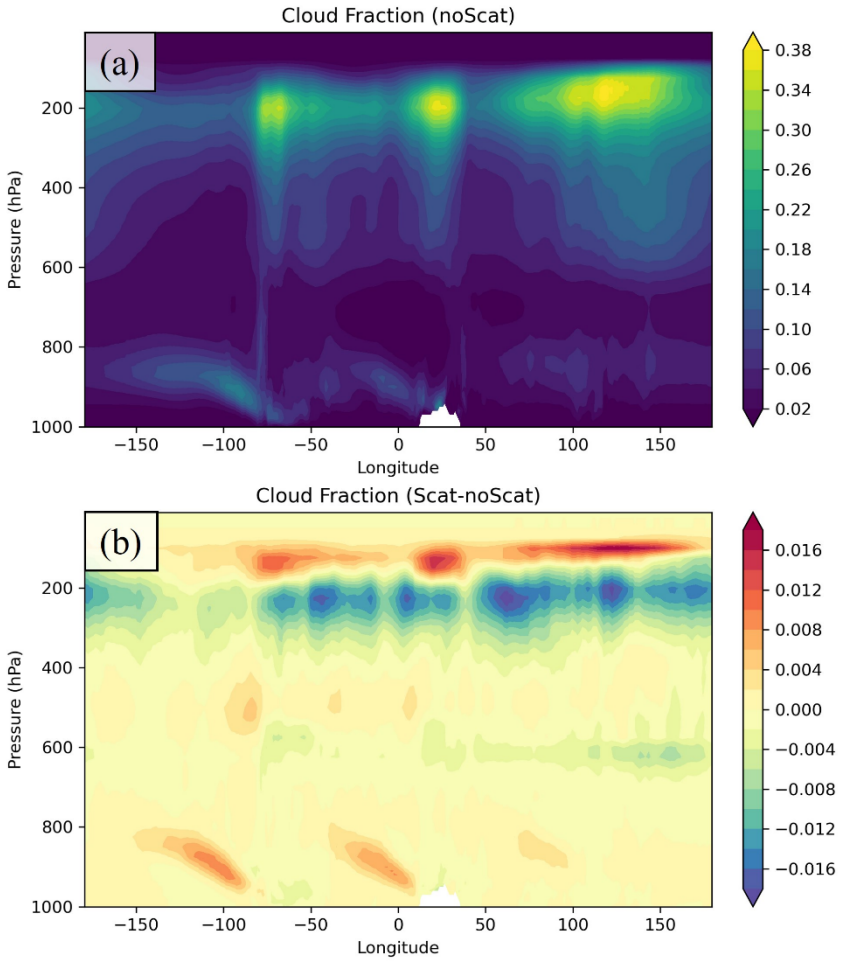

Figure 9. Longitude-pressure cross-section of (a) vertically-resolved cloud fraction averaged over the deep tropics (20ºS-20ºN) in the noScat run; and (b) Cloud fraction difference between the Scat run and the noScat run.

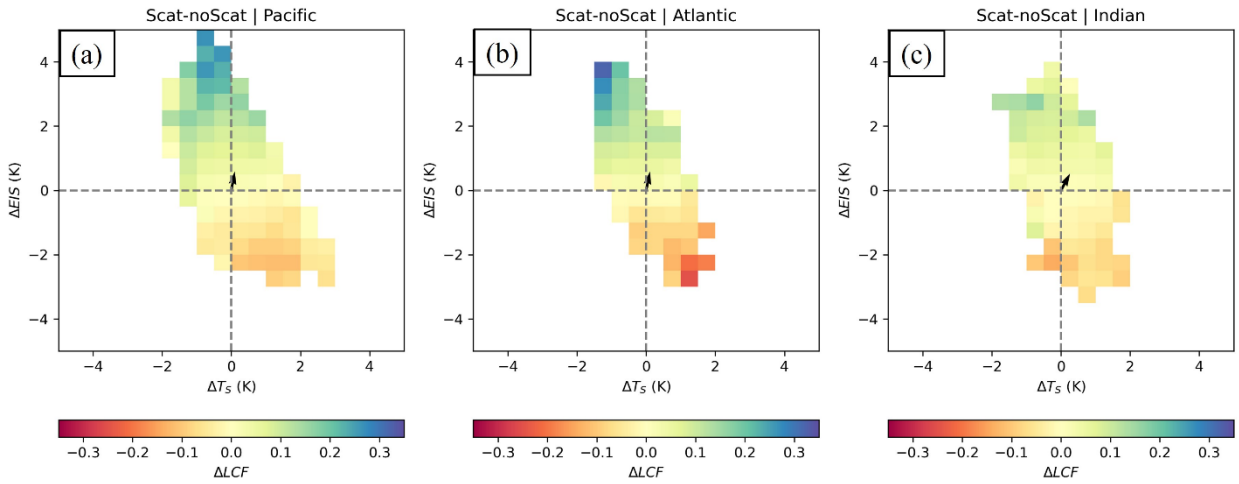

Figure 10. Monthly-mean low cloud fraction change binned by the surface temperature (T_S) change and the estimated inversion strength (EIS) change over three regions (a) southeastern tropical Pacific Ocean (120ºW~90ºW, 20ºS~10ºS), (b) southeastern tropical Atlantic Ocean (30Wº~0º, 20ºS~10ºS), and (c) southeastern tropical Indian Ocean (60ºE~80ºE, 20ºS~10ºS). The black solid vectors at the center of each panel show the long-term regional mean changes of EIS and T_S.

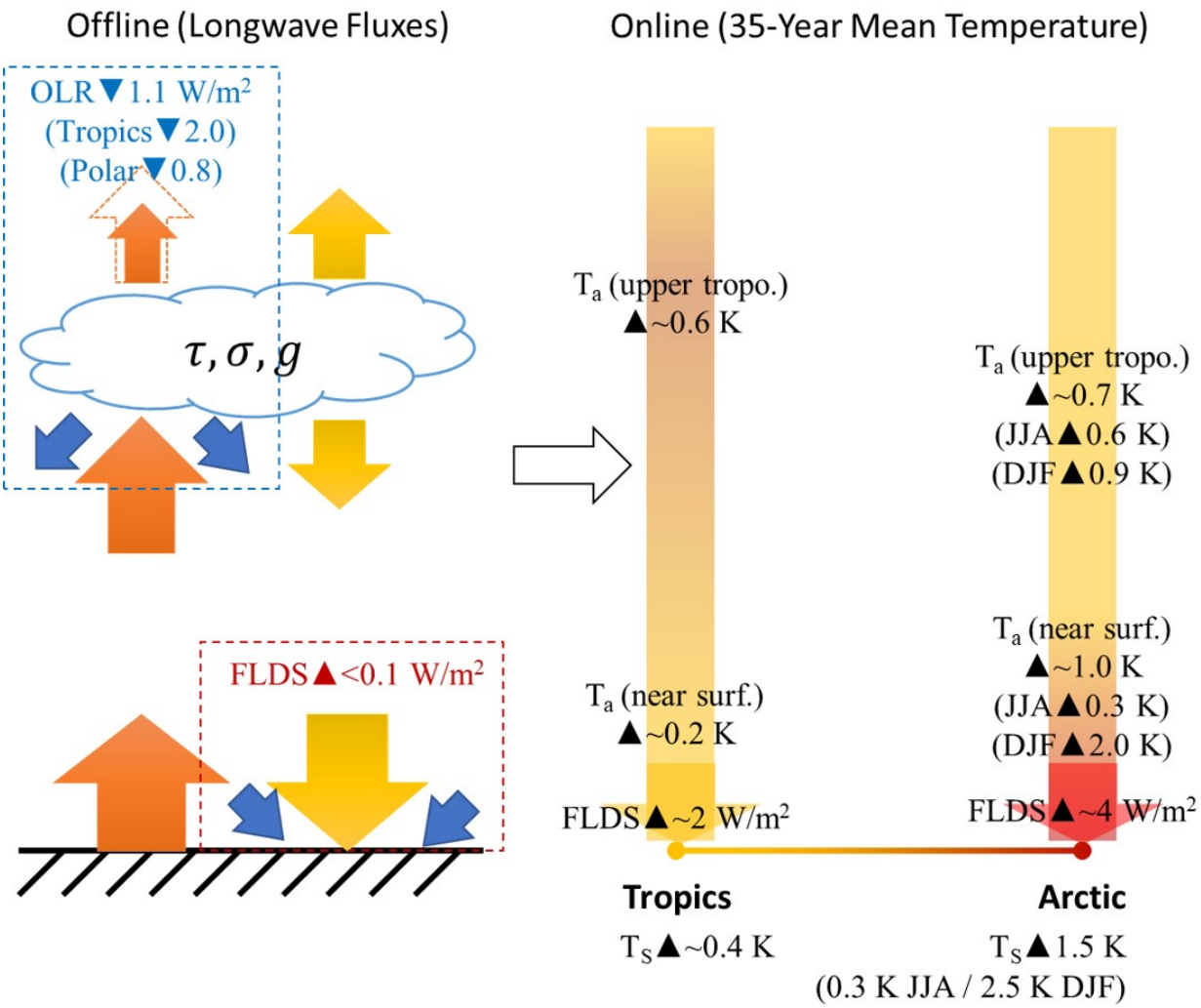

606

607 **Figure 11.** Schematic summary of the instantaneous radiative effect (left) and total temperature

608 responses (right) due to the cloud LW scattering effect. The results for the tropics and the Arctic

609 are shown separately.